

Choosing Appropriate Solvents for ASD Preparation

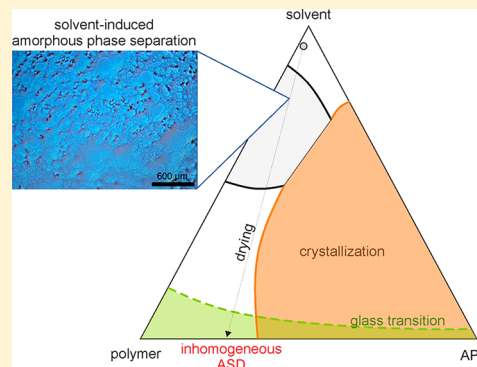
Christian Luebbert,^{ID} Daniel Real, and Gabriele Sadowski^{*ID}

Department of Biochemical and Chemical Engineering, Laboratory of Thermodynamics, TU Dortmund University, Emil-Figge-Str. 70, D-44227 Dortmund, Germany

Supporting Information

ABSTRACT: Amorphous solid dispersions (ASDs) are often used for formulating poorly water-soluble active pharmaceutical ingredients (APIs). In an ASD, the amorphous API is embedded in a suitable matrix excipient in order to stabilize the amorphous state and control the dissolution performance. ASDs can be prepared by commonly dissolving the API and the polymer in a suitable organic solvent which is evaporated afterward (e.g., via spray drying) aiming at a homogeneous API distribution in the polymer matrix. Sometimes, unexpected solvent influences on the heterogeneity of the dry ASD are observed. Thermodynamic predictions using the Perturbed-Chain Statistical Associating Fluid Theory combined with experimental investigations via Raman spectroscopy, differential scanning calorimetry, and microscopy performed in this work revealed the amorphous phase separation (APS) between the solvent and the polymer as causing the ASD heterogeneities. It will be shown that thermodynamic modeling allows for identifying appropriate solvents that will neither show APS with the polymeric excipient nor at any time of the drying process of ASD formulations.

KEYWORDS: *amorphous solid dispersion, amorphous phase separation, spray drying, organic solvent, homogeneity, PC-SAFT*



INTRODUCTION

Up to 90% of new active pharmaceutical ingredients (APIs) are poorly soluble in water,¹ assigned to Classes II and IV in the biopharmaceutical classification system. This poor water solubility leads to an insufficient bioavailability for the oral administration route and finally to rejection of potential API candidates during the development process. The state-of-the-art technique to overcome this solubility issue is the formulation of the API as an amorphous solid dispersion (ASD), in which the API is dissolved in a suitable polymer matrix forming a glassy solution.^{2–4} The polymer matrix is supposed to prevent the metastable amorphous API from unwanted crystallization during storage and controls the dissolution in aqueous media.^{4,5}

ASDs are prepared via solvent-free (e.g., hot-melt extrusion) or solvent-based methods (e.g., spray drying or film casting for screening purposes).^{4,6,7} Solvent-based formulation techniques are the method of choice for thermosensitive compounds and APIs with extremely high melting temperatures. In solvent-based processes, API and polymer are commonly dissolved in an organic solvent to obtain a homogeneous API/polymer/solvent solution. The organic solvent is thereafter removed by feeding the solution into a spray dryer in which the solvent evaporates immediately, leaving behind dry API/polymer particles.

Several works reported that the solvent decisively affects the product quality of a solvent-based formulation. Paudel et al. reported that the solvent used for spray drying of naproxen (NAP)/poly(vinylpyrrolidone) (PVP) ASDs influences the miscibility and physical stability of those formulations.⁸ Also

solvent mixtures were found to impact the final product quality. They performed thermodynamic calculations on the solvent-free binary system applying the Flory–Huggins theory, which of course could not explain the phenomena observed for different solvents.

The same authors found that quench-cooled films show different differential scanning calorimetry (DSC) thermograms (one glass-transition temperature) in measurements compared to solvent-casted films (two glass-transition temperatures). Costa et al. also found an unexpected solvent impact on the crystallinity of ASDs.⁹ Wu et al. found that the rate of solvent evaporation affects the long-term stability of piroxicam/PVP ASDs prepared from acetone/methanol mixtures.¹⁰ Wan et al. investigated particle properties and a drying process of spray-dried ASDs and found different release properties in spray-dried celecoxib/poly(lactic-*co*-glycolic acid) (PLGA) ASDs depending on the ratio of acetone to methanol in the applied solvent mixtures.¹¹

The reported results are remarkable, as all authors found differences in the product quality, product performance, and long-term stability of the ASDs depending on the choice of the organic solvent used for preparation. This seems to be surprising as the solvent is finally not present in the ASDs anymore. However, we will show in this work that thermodynamic phase diagrams of ternary API/polymer/

Received: August 23, 2018

Revised: October 8, 2018

Accepted: October 17, 2018

Published: October 17, 2018

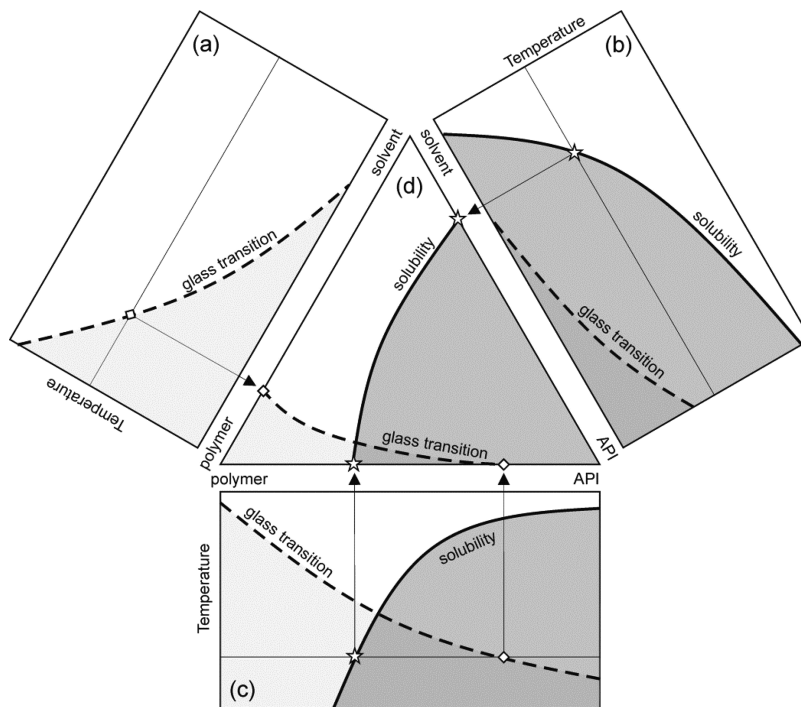


Figure 1. Schematic phase diagrams of mixtures showing no APS. Depicted are the binary systems (a) polymer/solvent, (b) solvent/API, (c) polymer/API, and (d) the ternary API/polymer/solvent mixture at a given temperature. The API solubility is depicted by black solid lines and the glass-transition temperature by dashed lines. Crystallization occurs in the dark gray areas, whereas light gray areas are regions below the glass-transition. The arrows connect the solubilities (stars) and glass-transition temperatures (diamonds) in the binary diagrams with the ones in the ternary diagram.

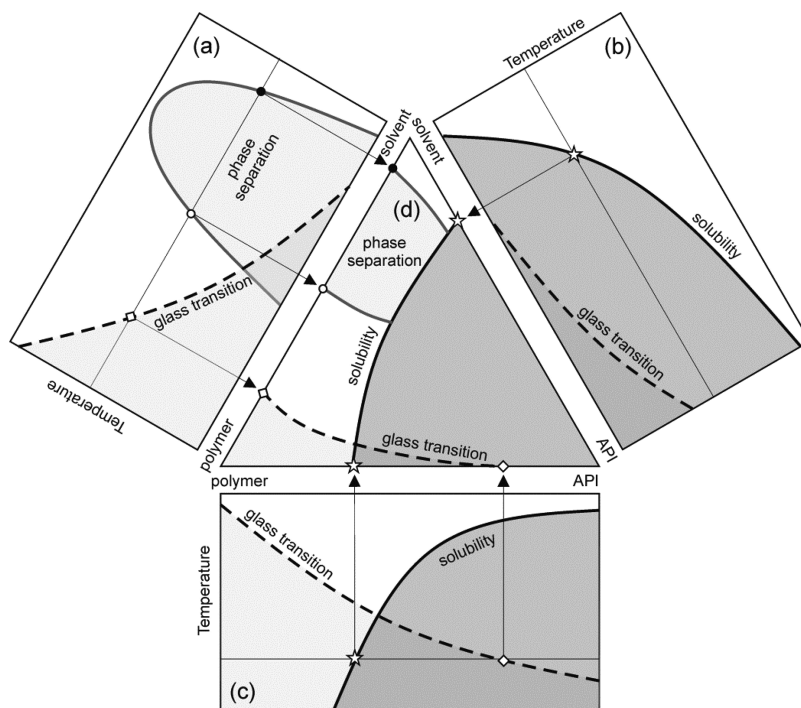


Figure 2. Schematic phase diagrams of mixtures showing APS. Depicted are the binary systems (a) polymer/solvent, (b) solvent/API, (c) polymer/API, and (d) the ternary API/polymer/solvent mixture at a given temperature. The API solubility is depicted by black solid lines, the border of the APS region by gray solid lines, and the glass-transition temperature by dashed lines. Crystallization occurs in the dark gray areas, APS in the gray areas, and the light gray areas are regions below the glass transition. The arrows connect the solubility (stars), APS (circles), and glass-transition temperatures (diamonds) in the binary diagrams with the ones in the ternary diagram.

solvent mixtures can provide a coherent explanation for these observations.

It is well-known, that many polymers undergo phase separation when mixed with solvents^{12–14} or other poly-

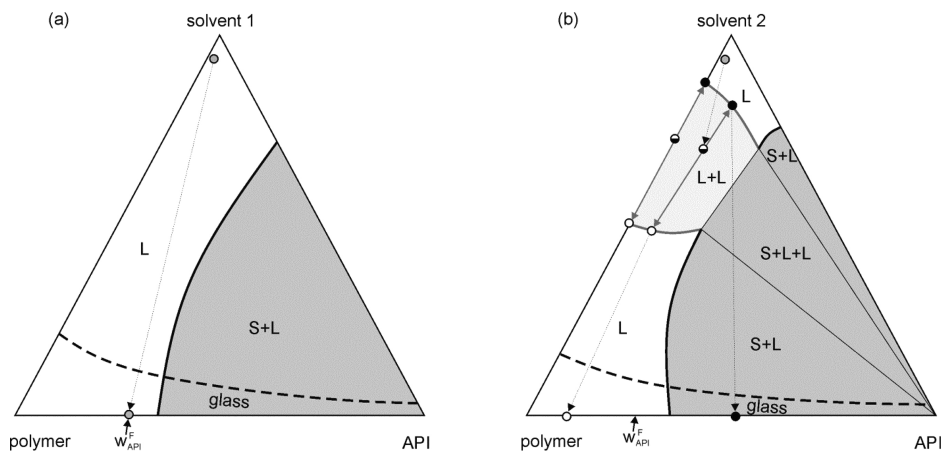


Figure 3. Phase diagram of a ternary API/polymer/solvent system (a) without APS and (b) with an APS region. The API solubility in the polymer/solvent mixture is depicted by black solid lines, the APS borders by gray lines, and the glass-transition by dashed lines. The ternary mixture is homogeneous in the white region (L), crystallization occurs in the dark gray areas (S+L and S+L+L), APS occurs in the gray areas (L+L and S+L+L), and the mixture is glassy below the dashed line. The gray circles mark the homogeneous solutions and the white and black circles are compositions of the separated phases. Arrows indicate the drying process of the ASD.

mers.^{15,16} The complex phase behavior of polymer/solvent systems has been characterized, e.g., for the design of polymer production processes.^{17,18} Many polymer/solvent mixtures are known to undergo phase separation (e.g., poly(ethylene glycol)/water¹⁹ or poly(lactic acid)/water²⁰). Phase separation in polymeric systems has been successfully described by thermodynamic models taking into account the complex polymer architecture and the chain-like structure, using the Flory–Huggins theory,²¹ the lattice–cluster theory,²² or the Perturbed-Chain Statistical Associating Fluid Theory (PC-SAFT).²³ PC-SAFT is a thermodynamic model applicable for describing phase equilibria (vapor sorption²⁴ and amorphous phase separation (APS)^{25,26}) in polymer/solvent mixtures,^{20,27} the solubility of APIs in organic solvents²⁸ and water,^{29,30} and the phase behavior of ASDs (solubility of APIs in polymers,³¹ APS,³² and the influence of moisture on solubility^{33,34} and APS^{35,36}). In this work, PC-SAFT is used to calculate phase equilibria in API/polymer/solvent mixtures and to gain, for the first time, a thermodynamic understanding of APS.

■ PHASE DIAGRAMS OF API/POLYMER/SOLVENT MIXTURES

Single-Solvent Systems. The phase diagram of the ternary API/polymer/solvent mixture can be derived from the phase diagrams of the binary subsystems,^{24,28,31,37–39} as depicted in Figure 1.

For a completely miscible polymer/solvent system (as shown in Figure 1a), the only relevant information is the glass-transition temperature. Due to the extremely low glass-transition temperatures of solvents (water, $-137\text{ }^\circ\text{C}$;⁴⁰ acetone, $-173\text{ }^\circ\text{C}$; ethyl acetate, $-155\text{ }^\circ\text{C}$;⁴¹ ethanol, $-177\text{ }^\circ\text{C}$; and isopropanol, $-175\text{ }^\circ\text{C}$;⁴²) the glass-transition temperature of polymer/solvent systems strongly decreases with increasing solvent content. The binary system API/solvent (Figure 1b) is characterized by the temperature-dependent solubility of crystalline API in the organic solvent. Similar to Figure 1a, the glass-transition temperature of this binary mixture drops from the value of the pure amorphous API (Figure 1b, right side) down to the value of the pure solvent. Figure 1c depicts the binary phase diagram of an API/polymer mixture, which was investigated in detail in earlier works.^{31,43,44}

Of main interest are again the glass transition of the ASD and the solubility of the API in the polymer.

The phase diagram of the ternary system API/polymer/solvent (Figure 1d) is directly obtained from Figure 1a–c by evaluating all three diagrams at the temperature of interest. The phase diagram for a system exhibiting solvent/polymer APS is shown in Figure 2.

The different shapes of the phase diagrams arise from the different phase behavior of the binary subsystems polymer/solvent (Figure 2a). While polymer and solvent were completely miscible in Figure 1a, they are only partly miscible in Figure 2a and thus exhibit an APS region. Polymer/solvent systems with compositions lying in this region will split up into two amorphous phases, one being solvent-rich (black circle in Figure 2a) and the other one being solvent-poor (white circle in Figure 2a). This miscibility gap pursues into the ternary API/polymer/solvent system (gray region in Figure 2d),^{13,14,45} meaning that all mixtures in this region will undergo APS. As the binary subsystems solvent/API (Figure 2b) and polymer/API (Figure 2c) are identical to Figure 1b,c, respectively, the absence or presence of an APS in the ternary system is only determined by the behavior of the polymer/solvent system in Figures 1a and 2a, respectively.

Figure 3 compares the ternary phase diagrams of systems showing no APS (Figure 3a compared to Figure 1d) with a system showing APS (Figure 3b compared to Figure 2d). Since they depict the same API/polymer mixture but with different solvents (solvent 1 not inducing APS and solvent 2 inducing APS), the binary API/polymer side looks the same for both diagrams.

The drying process of a hypothetical API/polymer/solvent mixture is indicated in both diagrams by arrows starting from a feed composition in the solvent-rich upper corner of the phase diagram running down to the solvent-free bottom side of the diagram. In an ideal drying process, as depicted in Figure 3a, the API solubility limit is never exceeded during drying, resulting in a homogeneous ASD without crystals or heterogeneities. In contrast, Figure 3b depicts the drying process in a mixture showing APS. In this case, the solvent-free bottom side of the phase diagram cannot be reached without crossing the APS region. Following the arrows in Figure 3b, the

initially homogeneous solution of API and polymer must cross the APS region upon drying. This means that the solution will split up along the arrows as soon as the drying mixture enters the APS region, leading to two phases exhibiting different API/polymer/solvent concentrations. These two phases continue drying independently. As they are extremely viscous or even below their glass-transition at the end of the drying process (bottom of the phase diagram), the thermodynamically preferred remixing will take quite some time (months or even years), leading to unwanted heterogeneous API-distribution in the dry ASD. In case the API-rich phase exceeds the equilibrium solubility, even unwanted crystallization may occur.

It is important to mention at that point, that phase separation will be observed only due to the choice of solvent 2, although the solvent-free ASD is fully miscible in thermodynamic equilibrium and thus expected to be homogeneous.

Mixed-Solvent Systems. In order to understand the ongoing phenomena during the preparation of ASDs using solvent mixtures, the APS region of the quaternary system API, polymer, solvent 1, and solvent 2 needs to be considered.

Figure 4 schematically shows the phase diagram of a quaternary mixture containing polymer, API, and two solvents.

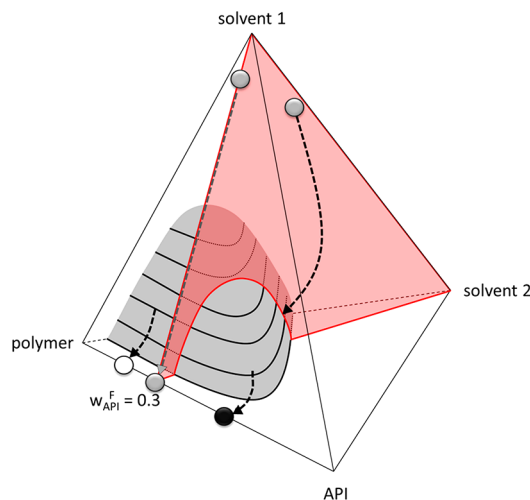


Figure 4. Schematic phase diagram of the system API/polymer/solvent 1/solvent 2 showing the APS region (gray) and one cut surface (red) for an ASD with $w_{\text{API}}^{\text{F}} = 0.30$. The route of drying is indicated by the dashed black line for a solvent 1/solvent 2 mixture and the dashed gray line for pure solvent 1, across which the ASD (circles) runs while drying. Homogeneous formulations are gray circles, and phase separated phases are black and white circles.

As depicted on the backside of the diagram, the binary polymer/solvent 2 subsystem undergoes APS, as already shown earlier in Figure 3b. All other binary subsystems polymer/solvent 1, API/solvent 2, solvent 1/solvent 2, and polymer/solvent 1 are completely miscible resulting in the APS region as depicted in Figure 4. The red area is the cut surface for one specific ASD drug loading in the ASD, e.g., $w_{\text{API}}^{\text{F}} = 0.30$.

As long as the mixture does not enter the APS region during the drying process, it will evolve along the red cut surface in Figure 4, since the API/polymer ratio remains constant during drying. However, since the two solvents usually differ in volatility, solvent 1 might evaporate first, causing the drying to not proceed along a straight line but along a bended line as

solvent 2 enriches in the liquid formulation compared to solvent 1. The section on the cut surface which intersects with the APS region is the so-called turbidity area, meaning that all mixtures within this area will phase separate,^{13,46} whereas for all other concentrations, APS can be successfully prevented.

During drying of a mixture with an API-to-polymer ratio of $w_{\text{API}}^{\text{F}} = 0.30$ prepared using a solvent 1/solvent 2 mixture (top point in Figure 4), the drying mixture crosses the APS region from the solvent-rich side of the diagram (right side) to the solvent-free corner of the diagram (bottom left side) and thus “enters” the APS region. APS occurs from now on, resulting into two phases with API/polymer ratios that not only differ from each other but also from the targeted one. Upon further drying the two phases leave the APS area at different positions (depicted by the two arrows at the left side of the APS surface) and finally result in a heterogeneous dry ASD. This could have been avoided by choosing a high excess of solvent 1 or even, as depicted by the black dashed arrow in Figure 4, pure solvent 1 based on the thermodynamic phase diagram of the API/polymer/solvent(s) system.

THEORY

Phase Equilibria. Phase separation into two amorphous (liquid) phases (referred to as L+L in Figure 4) occurs in systems with a phase behavior as depicted in Figures 3b and 4. This equilibrium is thermodynamically characterized by the equality of the chemical potentials of all three components i (API, polymer, and solvent) present in the two phases (L1 and L2) according to eq 1.

$$\mu_i^{\text{L1}} = \mu_i^{\text{L2}} \quad (1)$$

In this equation, μ_i^{L1} and μ_i^{L2} are the chemical potential of component i in the amorphous phases L1 and L2, respectively. This finally leads to the following phase equilibrium conditions where x_i is the mole fraction, and γ_i is the activity coefficient of component i.

$$x_{\text{API}}^{\text{L1}} \gamma_{\text{API}}^{\text{L1}} = x_{\text{API}}^{\text{L2}} \gamma_{\text{API}}^{\text{L2}} \quad (2)$$

$$x_{\text{polymer}}^{\text{L1}} \gamma_{\text{polymer}}^{\text{L1}} = x_{\text{polymer}}^{\text{L2}} \gamma_{\text{polymer}}^{\text{L2}} \quad (3)$$

$$x_{\text{solvent 1}}^{\text{L1}} \gamma_{\text{solvent 1}}^{\text{L1}} = x_{\text{solvent 1}}^{\text{L2}} \gamma_{\text{solvent 1}}^{\text{L2}} \quad (4)$$

$$x_{\text{solvent 2}}^{\text{L1}} \gamma_{\text{solvent 2}}^{\text{L1}} = x_{\text{solvent 2}}^{\text{L2}} \gamma_{\text{solvent 2}}^{\text{L2}} \quad (5)$$

According to eqs 2–5, four components are in equilibrium in the phases L1 and L2 (API, polymer, solvent 1, and solvent 2). Eqs 2–5 need to be solved simultaneously to obtain two corresponding points (connected by tie lines) of the APS regions shown in Figures 3b and 4.

The solubility of a crystalline API in a solvent, a polymer, or a mixture thereof is characterized by the equilibrium between the amorphous phase (L) and the crystalline API phase (solid, S) (Figures 1, 2, and 3). API is present in both phases, while polymer and solvent are only present in the amorphous phase. Therefore, only the chemical potential of the API in phases L and S needs to be considered for the equilibrium calculation according to eq 6.

$$\mu_{\text{API}}^{\text{L}} = \mu_{\text{API}}^{\text{S}} \quad (6)$$

Assuming that the API crystallizes pure and without solvate formation, eq 6 can be rewritten as given by eq 7.⁴⁵

$$x_{\text{API}}^{\text{L}} = \frac{1}{\gamma_{\text{API}}^{\text{L}}} \exp \left\{ -\frac{\Delta h_{\text{API}}^{\text{SL}}}{RT} \left(1 - \frac{T}{T_{\text{API}}^{\text{SL}}} \right) - \frac{\Delta c_{\text{p,API}}^{\text{SL}}}{R} \right. \\ \left. \left[\ln \left(\frac{T_{\text{API}}^{\text{SL}}}{T} \right) - \frac{T_{\text{API}}^{\text{SL}}}{T} + 1 \right] \right\} \quad (7)$$

This equation describes the mole fraction solubility of the API in ($x_{\text{API}}^{\text{L}}$) as a function of temperature T and requires the API melting properties $\Delta h_{\text{API}}^{\text{SL}}$ (melting enthalpy of the API), $\Delta c_{\text{p,API}}^{\text{SL}}$ (heat capacity difference between crystalline and liquid API), and $T_{\text{API}}^{\text{SL}}$ (melting temperature of the API) obtained from DSC measurements and the ideal gas constant ($R = 8.3145 \text{ J/(mol}\cdot\text{K)}$). The S+L+L area in Figure 3b is determined by simultaneously solving eqs 2–5 and 7.

Information about the interactions between the polymer and the solvent(s) is obtained in this work from experimental vapor-sorption equilibrium data. They can be modeled via the following equilibrium condition

$$x_{\text{solvent}}^{\text{L}} \gamma_{\text{solvent}}^{\text{L}} = a_{\text{solvent}}^{\text{L}} = \frac{p_{\text{solvent}}}{p_{0,\text{solvent}}^{\text{LV}}} \quad (8)$$

whereas p_{solvent} is the partial pressure of the solvent, and $p_{0,\text{solvent}}^{\text{LV}}$ is the vapor pressure of the pure solvent at a given temperature. The ratio of these two equals the solvent activity in the liquid phase $a_{\text{solvent}}^{\text{L}}$, which is the product of the solvent mole fraction concentration in the liquid phase $x_{\text{solvent}}^{\text{L}}$ and activity coefficient of the solvent in the liquid phase $\gamma_{\text{solvent}}^{\text{L}}$. The activity coefficients required in eqs 2–5, 7, and 8 account for the nonidealities in mixtures of API, polymer, and solvent(s) and are obtained in this work from the PC-SAFT model.

Glass-Transition Temperatures. The glass transition of API/polymer/solvent mixture is a measure for the kinetic stability of an ASD and was predicted in this work using the Gordon–Taylor equation for ternary systems⁴⁷ according to eq 9.

$$T_g = \frac{w_{\text{polymer}}^{\text{L}} T_{g,\text{polymer}} + K_{\text{polymer,API}} w_{\text{API}}^{\text{L}} T_{g,\text{API}} + K_{\text{polymer,solvent}} w_{\text{solvent}}^{\text{L}} T_{g,\text{solvent}}}{w_{\text{polymer}}^{\text{L}} + K_{\text{polymer,API}} w_{\text{API}}^{\text{L}} + K_{\text{polymer,solvent}} w_{\text{solvent}}^{\text{L}}} \quad (9)$$

In this equation, the mass fractions of the amorphous API, polymer, and solvent are abbreviated as $w_{\text{API}}^{\text{L}}$, $w_{\text{polymer}}^{\text{L}}$, and $w_{\text{solvent}}^{\text{L}}$, respectively. $T_{g,\text{API}}$, $T_{g,\text{polymer}}$, and $T_{g,\text{solvent}}$ are the glass-transition temperatures of the pure compounds, and $K_{\text{polymer,API}}$ and $K_{\text{polymer,solvent}}$ are the Gordon–Taylor interaction parameters between polymer/API and polymer/solvent, respectively. These parameters were estimated in this work by the following expression (eq 10).

$$K_{\text{polymer,API}} = \frac{\rho_{\text{polymer}} T_{g,\text{polymer}}}{\rho_{\text{API}} T_{g,\text{API}}}; \quad K_{\text{polymer,solvent}} = \frac{\rho_{\text{polymer}} T_{g,\text{polymer}}}{\rho_{\text{solvent}} T_{g,\text{solvent}}} \quad (10)$$

The densities of the amorphous polymer, API, and solvent (ρ_{polymer} , ρ_{API} , and ρ_{solvent}) and the T_g temperatures [K] were taken from literature and are summarized in Table 1.

PC-SAFT. Activity coefficients are crucial for the thermodynamic calculation of APS (eqs 2–5), solubility (eq 7), and solvent sorption (eq 8). They were obtained in this work from the residual Helmholtz energy a^{res} . According to PC-SAFT,^{23,25} a^{res} is calculated as the sum of contributions accounting for different intermolecular interactions, namely, a hard chain repulsion a^{hc} , van der Waals dispersion forces a^{disp} , and hydrogen-bonding a^{assoc} , as shown in eq 11.

Table 1. Densities, Melting Properties, and Glass-Transition Temperatures of the Substances Investigated in This Work

	(ρ kg/m ³)	T_g (°C)	T^{SL} (°C)	Δh^{SL} (kJ/mol)	Δc_p^{SL} (J/(mol·K))
PVP	1250 ^a	168.4 ^b			
NAP	1250 ^c	-8 ^b	156.32 ^d	31.50 ^d	87.44 ^d
felodipine	1280 ^e	46.6 ^f	143.70 ^f	30.83 ^e	89.87 ^f
acetone	790 ^g	-173.0 ^h			
ethanol	790 ^g	-177.0 ⁱ			
DCM	1330 ^g	-170.1 ^h			

^aRef 48. ^bRef 43. ^cRef 49. ^dRef 50. ^eRef 51. ^fRef 32. ^gDensity at 20 °C. ^hRef 41. ⁱRef 42.

$$a^{\text{res}} = a^{\text{hc}} + a^{\text{disp}} + a^{\text{assoc}} \quad (11)$$

Five pure-component parameters are used to characterize a molecule, which is described as a chain of m^{seg} spherical segments with diameter σ . For polymers, usually the parameter m^{seg}/M (M being the molecular weight of the polymer) is used, which does not depend on the polymer molecular weight and thus easily allows predicting the thermodynamic behavior for different polymer chain lengths. The dispersion energy u/k_B (k_B is the Boltzmann constant) is a measure for the van der Waals interactions. Hydrogen bonds in associating components exhibiting N^{assoc} association sites are characterized by the association energy $\varepsilon^{\text{AB}}/k_B$ and the association volume κ^{AB} . Pure-component parameters for all components investigated in this work were already reported in literature and are summed up in Table 2.

In mixtures, Berthelot-Lorentz mixing rules are applied to calculate σ_{ij} (eq 12) and u_{ij} (eq 13). Wolbach and Sandler mixing rules⁵⁵ are applied for determining the cross-association parameters $\varepsilon^{\text{AiBj}}$ (eq 14) and κ^{AiBj} (eq 15).

$$\sigma_{ij} = \frac{1}{2}(\sigma_i + \sigma_j) \quad (12)$$

$$u_{ij} = (1 - k_{ij}) \sqrt{u_i u_j} \quad (13)$$

$$\varepsilon^{\text{AiBj}} = \frac{1}{2}(\varepsilon^{\text{AiBi}} - \varepsilon^{\text{AjBj}}) \quad (14)$$

$$\kappa^{\text{AiBj}} = \sqrt{\kappa^{\text{AiBi}} \kappa^{\text{AjBj}}} \left(\frac{\sqrt{\sigma_i \sigma_j}}{\frac{1}{2}(\sigma_i + \sigma_j)} \right)^3 \quad (15)$$

The interaction parameter k_{ij} between components i and j (eq 13) corrects for the dispersion between unlike molecules and is fitted to any easily assessable, experimental data of the binary system (e.g., the API solubility in a solvent, solvent vapor sorption in the polymer, or APS in polymer/solvent systems). Experimental solubilities of APIs in organic solvents which were not available from literature were determined in this work and are given in the Supporting Information. The accuracy of the PC-SAFT modeling was quantified by the maximum relative deviation (MRD) and average relative deviation (ARD), calculated according to eqs 16 and 17.

$$\text{MRD} = 100 \max_{i=1, n_{\text{exp}}} \left| \frac{\Omega_{\text{calc},i} - \Omega_{\text{exp},i}}{\Omega_{\text{exp},i}} \right| \quad (16)$$

Table 2. PC-SAFT Pure-Component Parameters of the Investigated Compounds

	<i>M</i> (g/mol)	<i>m</i> ^{seg} / <i>M</i> (mol/g)	σ (Å)	<i>u/k</i> _B (K)	$\epsilon^{AB}/kB (K)$	κ^{AB}	<i>N</i> ^{assoc}
FEL ^a	384.26	0.0300	3.205	234.543	1581.1	0.02	2/2
NAP ^b	230.26	0.0352	2.939	229.450	934.2	0.02	2/2
PVP ^b	25700	0.0407	2.710	205.599	0	0.02	231/231
acetone ^c	58.08	0.0498	3.228	247.42	0	0.01	1/1
DCM ^d	84.93	0.0266	3.338	274.20			
ethanol ^e	46.07	0.0517	3.1771	198.24	2653.4	0.032384	1/1

^aRef 32. ^bRef 43. ^cRef 52. ^dRef 53. ^eRef 54.**Table 3.** PC-SAFT Binary Interaction Parameters (k_{ij}) between the Investigated Compounds

	k_{ij}	type of data used for fitting	temperature range (°C)	ARD (%)	MRD (%)
PVP/ethanol	-0.070	sorption	25	2.3	7.5
PVP/acetone	0.0113	APS (PVP-rich phase)	15–35	2.4	3.7
PVP/NAP ^a	0.000128 T [K] - 0.1297	solubility			
PVP/FEL ^b	0.030	solubility			
PVP/DCM	-0.042	sorption	25	5.9	11.2
FEL/acetone	-0.000065 T [K] + 0.0273	solubility	15–40	4.0	13.5
FEL/ethanol ^c	0.000034 T [K] - 0.0097	solubility			
NAP/acetone	-0.0045	solubility	25	<i>f</i>	<i>f</i>
NAP/ethanol ^d	-0.000135 T [K] + 0.0394	solubility			
NAP/DCM	0.01126	solubility	25	<i>f</i>	<i>f</i>
DCM/ethanol ^e	-0.01	vapor–liquid			

^aRef 43. ^bRef 35. ^cRef 32. ^dRef 56. ^eRef 57. *f*Fit to only one data point.

$$ARD = 100 \frac{1}{n_{exp}} \sum_{i=1}^{n_{exp}} \left| \frac{\Omega_{calc,i} - \Omega_{exp,i}}{\Omega_{exp,i}} \right| \quad (17)$$

Eqs 16 and 17 compare the calculated values (Ω_{calc}) with the experimental values (Ω_{exp}), n_{exp} is the number of experimental data points. The obtained k_{ij} -values, the type of data used for their fitting, as well as the ARD/MRD values are summed up in Table 3.

All thermodynamic equilibria (APS, solubility, and vapor-sorption) were calculated with the same set of pure-component parameters given in Table 2 and the binary interaction parameters from Table 3.

EXPERIMENTS

Materials. FEL (purity 99.7%) was purchased from Discovery Fine Chemicals (Wimborne, United Kingdom), and NAP (purity >99%) was obtained from TCI Deutschland (Eschborn, Germany). The polymer PVP (Kollidon K2S, molecular weight of 25 700 g/mol) was obtained from BASF (Ludwigshafen, Germany). The solvents ethanol (purity 99%), acetone (purity 99.9%), and dichloromethane (DCM, purity 99.8%) were supplied by VWR International (Darmstadt, Germany). Solvents used for vapor-sorption experiments were degassed by successive freezing in liquid nitrogen, evacuation, and melting under vacuum conditions, and PVP was stored under vacuum conditions to avoid moisture absorption.

Quantification of APS in Binary Polymer/Solvent Mixtures. The equilibrium APS concentrations of binary polymer/solvent mixtures were determined in a stirred, temperature-controlled (accuracy ± 0.1 K) glass vessel. Polymer solutions with feed concentrations in the APS region were prepared and stirred for at least 24 h. The two coexisting liquid phases were separated, and samples were withdrawn from both phases. The solvent concentrations in both phases were measured gravimetrically (accuracy ± 0.1 mg) by

determining the mass loss after drying under vacuum conditions for 1 week.

Preparation of ASDs. The ASDs investigated in this work were prepared by solvent evaporation. In total, 500 mg of API and polymer were weighted in the desired API/polymer ratio on an analytical lab balance (accuracy ± 0.1 mg) and dissolved in 5 mL of solvent. API and polymer were completely dissolved in the case of using ethanol and acetone/DCM mixtures, and a turbid solution was obtained from the acetone mixtures. Solutions were casted on glass slides to obtain ASD films. Solvent was evaporated under visual observation during a primary drying step at standard laboratory conditions (25 °C). Spray-dried ASDs were prepared with a Büchi B290 lab-scale spray dryer (Flawil, Switzerland) operated at an aspirator temperature of 60 °C. The aspirator power was set to 100%, the feed solution was fed with a pump rate of 8 mL/min, and 550 L/h technical nitrogen was used for atomizing the feed solution and inerting the whole spray dryer. Independent of the chosen preparation procedure, a further drying step was conducted in a vacuum oven operated at 25 °C to remove residual solvent.

Vapor-Sorption Experiments. The organic-vapor-sorption in PVP was measured with a Rubotherm magnetic suspension balance (Bochum, Germany) with an accuracy of ± 0.03 mg, the setup of the apparatus was already described earlier.⁵⁸ Pure degassed solvent was fed from a vaporizer to the temperature-controlled measurement cell. The vapor uptake was monitored gravimetrically for different vapor partial pressures (eq 8) to determine the sorption isotherm.

Investigation of Sample Homogeneity. Sample homogeneity was investigated microscopically in film-casted ASDs using a Leica DM400 M microscope (Wetzlar, Germany), by which the sample appearance and qualitative presence of droplet-like structures were determined.

Raman measurements were carried out to quantify the API distribution in the films and to investigate the compositions in

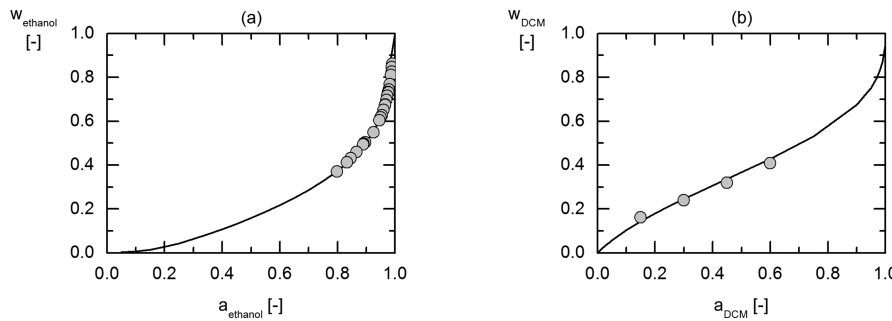


Figure 5. Vapor-sorption isotherms of the systems (a) PVP ($M_w = 10,000 \text{ g/mol}$)/ethanol at 25 °C and (b) PVP K25 ($M_w = 25,700 \text{ g/mol}$)/DCM at 25 °C. The symbols are experimental data (PVP/ethanol data points from ref 61 and PVP K25/DCM measured in this work), and lines are PC-SAFT calculations using eq 8.

the films during drying.³⁶ Measurements were carried out on a HORIBA LabRAM Raman spectrometer (Bensheim, Germany) connected to an Olympus IX71 inverted microscope (Tokyo, Japan). The confocal pinhole of the apparatus was set to 200 μm , the used grating had 600 grooves/mm, and the intensity of the 532 nm laser (300 mW power) was reduced by a gray filter to avoid sample degradation. Each Raman spectrum was the average of two measurements with a counting time of one second. Raman spectra were quantified with the indirect hard modeling method^{59,60} implemented in the PEAXACT 4.0 software by s-PACT (Aachen, Germany). Calibrations were carried out with at least four spectra of each binary mixture. DSC measurements were performed on a TA Instruments Q2000 device (New Castle, DE, USA), which was temperature calibrated using indium. Approximately 10 mg of the ASD were transferred into standard pans with a pinhole lid and investigated in the temperature range from 20 to 180 °C with a modulated heating ramp of 2 °C/min (heating-only procedure; heat amplitude of 0.318 K at a period of 60 s). The ASDs were investigated in a heat-cool-heat procedure as described in earlier works.^{31,32}

RESULTS

Phase Diagrams of Polymer/Solvent Systems. Experimental data for solvent vapor sorption in PVP were used for fitting the binary PC-SAFT parameters for fully miscible polymer/solvent mixtures (Table 3). Figure 5 shows the obtained vapor-sorption isotherms of PVP/ethanol and PVP K25/DCM mixtures.

The vapor sorption of ethanol in PVP ($M_w = 10,000 \text{ g/mol}$) was determined experimentally by Zafarani-Moattar and Samadi⁶¹ (Figure 5a) for high ethanol activities $0.80 < a_{\text{ethanol}} < 0.99$. In that range, the mass fraction of absorbed ethanol exponentially increases from 0.37 to 0.86. Figure 5b shows the results for the DCM-sorption experiment in PVP K25 conducted in this work for DCM activities in the range $0.15 \leq a_{\text{DCM}} \leq 0.60$. It can be seen, that the absorbed DCM mass fraction increases from 0.162 to 0.408 in the investigated range.

The sorption isotherms for both systems can be described by PC-SAFT in quantitative agreement with the experimental data using the fitted k_{ij} values reported in Table 3 (ARD = 2.3% in PVP/ethanol and ARD = 5.9% in PVP/DCM). It needs to be noted, that k_{ij} does not depend on the molecular weight of a polymer and can thus be used for PVPs of different molecular weights.²⁵ Simultaneously solving eqs 2–4 using the parameters from Tables 2 and 3 revealed that there is no APS in these two systems, which exactly corresponds to the

experimental findings. Thus, DCM and ethanol are regarded as “appropriate” solvents for preparing ASDs with PVP, as they do not show APS.

In contrast, the mixture of PVP/acetone was PC-SAFT-predicted to show APS and is thus regarded as being “inappropriate” for the preparation of PVP-containing ASDs. In order to characterize the APS region of this mixture, acetone and PVP were mixed in a weight ratio acetone:PVP = 4:1. Two liquid phases evolved. The amount of PVP in both phases was determined by measuring gravimetrically the weight loss of the two phases after drying, the results of the measurements are depicted in Figure 6.

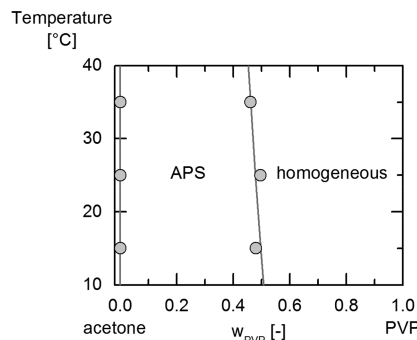


Figure 6. APS region of the system PVP/acetone. Symbols are experimental data points determined in this work, and the lines are PC-SAFT calculations using eqs 2 and 3 and the parameters in Tables 2 and 3.

As shown in Figure 6, PVP concentrations in the phase-separated PVP/acetone mixtures were determined at the temperatures 15, 25, and 35 °C. At 25 °C, the acetone-rich phase contained gravimetrically not-detectable amounts of PVP ($w_{\text{PVP}} \approx 0.0$), while the coexisting acetone-lean phase contained $w_{\text{PVP}} = 0.485$ PVP. It was found that the temperature shift down to 15 °C and up to 35 °C did not remarkably affect the width of the APS region. In perfect agreement to the measured data, PC-SAFT quantitatively correctly describes both, the acetone-lean and the acetone-rich phases.

Phase Separation in API/Polymer/Solvent Systems. Predicted Phase Diagrams. Ternary phase diagrams of API/PVP/solvent mixtures were predicted using eqs 2–4 to explore the development of APS during the ASD drying process. The results of those predictions are shown in Figure 7.

Figure 7a,b shows the PC-SAFT-predicted phase diagrams for the mixtures NAP/PVP/ethanol and NAP/PVP/acetone at 25 °C, respectively. The only difference between these two is

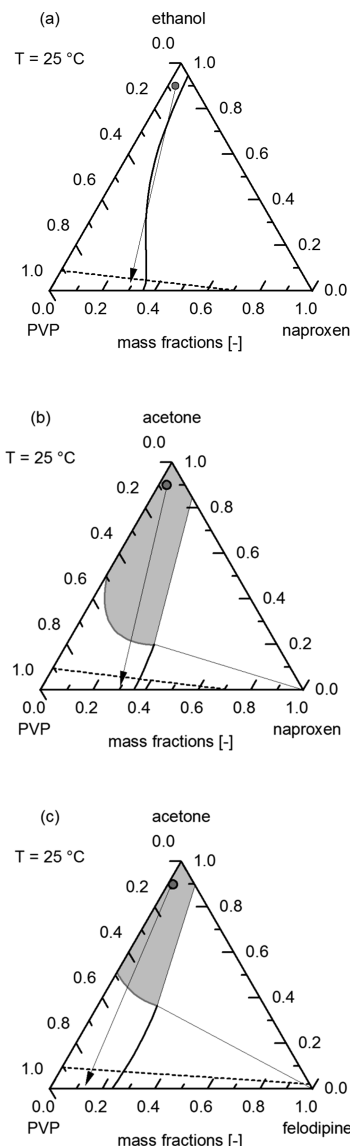


Figure 7. Predicted phase diagrams of the systems (a) NAP/PVP/ethanol, (b) NAP/PVP/acetone, and (c) FEL/PVP/acetone at 25 °C. Black lines represent the PC-SAFT-predicted crystalline-API solubility in the solvent/polymer mixture, and the gray region is the PC-SAFT-predicted APS region. The glass-transition of the mixture was predicted to be 25 °C along the dashed line. The drying processes of the initial mixture (gray circles) are indicated by the thin arrows.

the solvent, ethanol in Figure 7a and acetone in Figure 7b. According to Figure 7a, no APS region is predicted for the ethanol system, and thus it is expected that the mixture with ethanol will not undergo APS during the drying process as indicated by the arrow. As the arrow (very) slightly intersects with the solubility line, crystallization might occur during evaporation. However, this is not a general concern for all evaporation processes and depends on the course of the solubility line. Moreover, this particular system crystallization was not experimentally observed (probably due to the very low supersaturation). For the acetone system (Figures 7b), PC-SAFT predicts an APS region becoming even wider with increasing NAP content in the mixture. Starting from the solvent-rich corner of the diagram (the starting point is indicated by the gray circle in Figure 7), it is impossible to reach the bottom side of the phase diagram without crossing the APS region. This means that PC-SAFT predicts that APS will occur during drying. The glass-transition is not affected by the solvent because both solvents have similar glass-transition temperatures and densities (Table 1).

The influence of different APIs can be studied by comparing Figure 7b and Figure 7c. This time, the polymer and solvent are the same (PVP/acetone), and NAP is compared to FEL. According to the PC-SAFT predictions, the shape of the APS region is significantly affected by the API; the width of the APS region does not increase in the presence of FEL (Figure 7c) as it does for the NAP containing system (Figure 7b). This arises from the different intermolecular interactions in the API/polymer/solvent system, as accounted for by PC-SAFT. However, the left side of the triangle diagram (polymer/solvent binary) is not affected by the API, and thus APS occurs regardless of the API.

Experimental Findings. NAP/PVP ASDs with an NAP content of $w_{\text{NAP}}^{\text{F}} = 0.30$ in the solvent-free ASD ($w_{\text{API}}^{\text{F}} = \frac{w_{\text{API}}}{w_{\text{API}} + w_{\text{polymer}}}$) were prepared via solvent evaporation, as described in the Preparation of ASDs section, with one using ethanol and one using acetone. According to the PC-SAFT modeling of the water-free NAP/PVP mixture already performed in the work of Prudic et al.,⁴³ the solubility of NAP in solvent-free PVP is $w_{\text{NAP}}^{\text{F}} = 0.356$ (compare Figure 7a and Figure 7b), meaning that an ASD with NAP $w_{\text{NAP}}^{\text{F}} = 0.30$ is finally thermodynamically stable regardless of the chosen solvent and regardless of the preparation method. However, thermodynamic equilibrium will only be reached after infinite time. If the solvent induces APS during drying, it will influence the phase behavior of the ASD formulations at intermediate

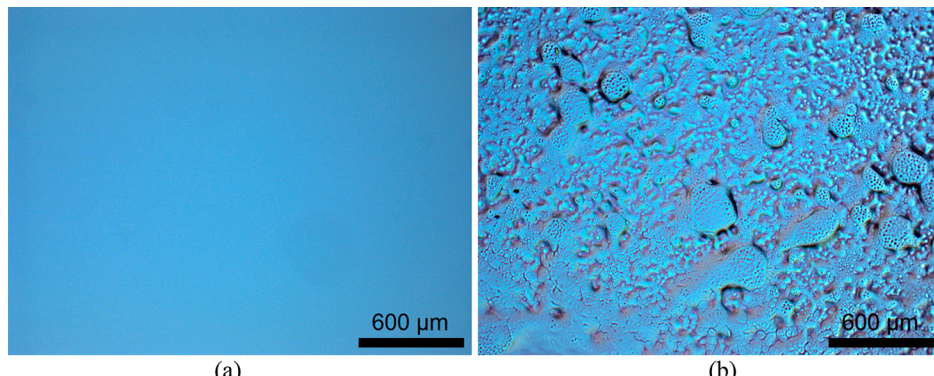


Figure 8. Microscopic images of NAP/PVP films prepared via solvent-evaporation using the solvents (a) ethanol and (b) acetone.

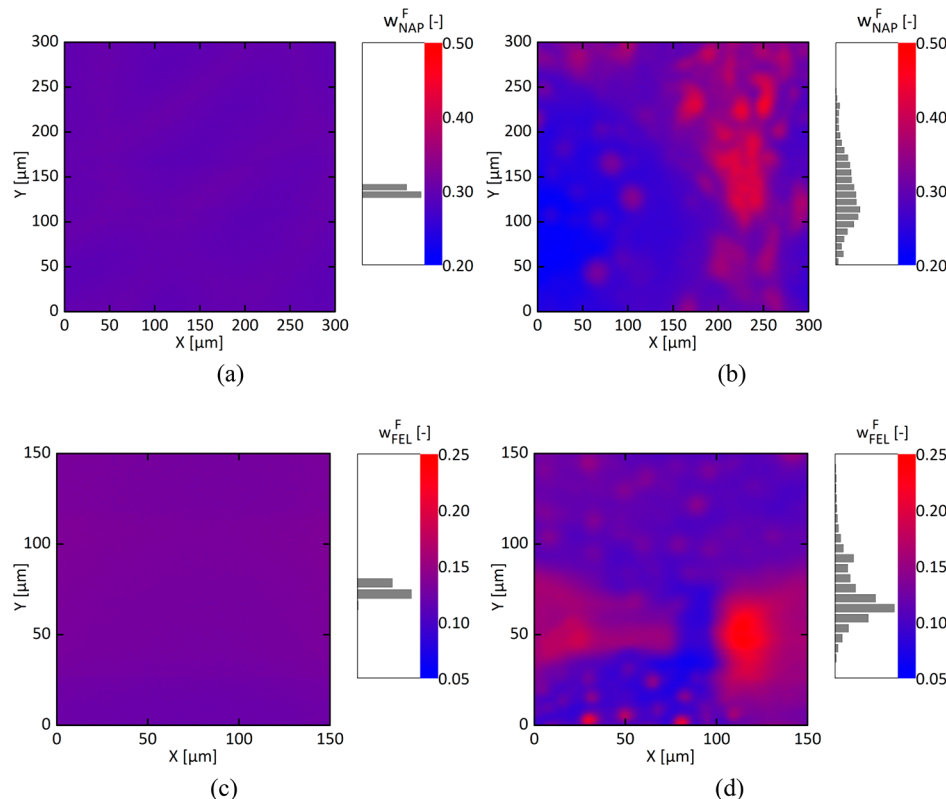


Figure 9. Raman maps of solvent-evaporated ASDs investigating the API distribution in the polymer matrix after the solvent evaporation process. (a, b) NAP/PVP ASDs and (c, d) FEL/PVP ASDs prepared using either the solvent ethanol (a, c) or acetone (b, d). The relative spectrum distribution is given at the side of each map.

time steps. This is shown in Figure 8 by means of microscopic images of the resulting ASDs using ethanol and acetone.

As can be seen from Figure 8a, the preparation of the NAP/PVP ASD using ethanol yields a perfectly clear and homogeneous film. In contrast, Figure 8b shows the resulting ASD prepared using acetone as solvent. The entire formulation contained droplet-like structures, and also the initial NAP/PVP/acetone solution was not clear but turbid.

Raman maps were conducted to quantitatively investigate the API distribution in the resulting ASDs.

Figure 9 shows the Raman maps of NAP/PVP (a,b) and FEL/PVP (c,d) ASDs prepared using either ethanol or acetone. In the NAP/PVP ASD prepared from ethanol (Figure 9a), the measured NAP content shows the same value ($w_{\text{NAP}} = 0.30$) throughout the entire investigated area ($300 \mu\text{m} \times 300 \mu\text{m}$), which coincides perfectly with the initial starting composition. No concentration fluctuations were observed in this area, as already expected from the phase behavior in Figure 8. In contrast to that, Figure 9b shows the Raman map of an NAP/PVP ASD prepared using acetone. In this map, droplet-like regions with higher NAP content were observed. The NAP concentrations were observed to vary between $w_{\text{NAP}} = 0.205$ and $w_{\text{NAP}} = 0.445$. Now, a dramatic heterogeneity prevails in the ASD, and the separated phases obviously did not remix when leaving the APS region in the phase diagram and reaching the thermodynamically preferred one-phase region (Figure 7b) at the end of the drying process. This can be explained by the very slow remixing kinetics resulting from the extremely high viscosity of the ASD below the glass-transition temperature (see also Figure 7b). In addition to this heterogeneity, the NAP-rich compartments in the ASD now

exceed the solubility limit of NAP in PVP ($w_{\text{NAP}} = 0.356$), meaning that crystals might evolve in these parts of the ASD.

Similar observations were made for FEL/PVP ASDs with $w_{\text{FEL}} = 0.13$. While ethanol yielded a completely homogeneous ASD (Figure 9c) without concentration fluctuations, acetone again caused a heterogeneous API distribution in the polymer matrix (Figure 9d), now with FEL concentrations lying in the range $0.068 \leq w_{\text{FEL}} \leq 0.237$. Irrespective of the chosen API, APS dramatically impairs the heterogeneity and the product quality of an ASD.

Phase Separation in Systems of API/Polymer/Mixed Solvents. Predicted Phase Diagram. The APS region in the system NAP/PVP/acetone/DCM with an NAP content of $w_{\text{NAP}}^{\text{F}} = 0.30$ in the solvent-free system was predicted using the PC-SAFT parameters from Tables 2 and 3 and is depicted in Figure 10.

Figure 10 shows the PC-SAFT-calculated APS region for an NAP/PVP ASD with $w_{\text{NAP}}^{\text{F}} = 0.30$ in a mixture of acetone and DCM. Moreover, this diagram contains *in situ* (via Raman microscopy)-determined experimental concentrations in a solvent-casted film during the drying process, which will be discussed in the next section. The solution was observed to be clear at the beginning of the experiment and thus lied in the homogeneous region, meaning that PC-SAFT seems to slightly overestimate the size of the APS region in Figure 10. The binary systems acetone/DCM and ASD/DCM are fully miscible as can be seen from the respective sides of the triangle (the left border of the APS region does not cross the $w_{\text{ASD}} = 0.0$ line). The APS starts in the DCM-free acetone/ASD system and becomes narrower (miscibility increases) with increasing DCM content in the mixture. APS can be avoided as

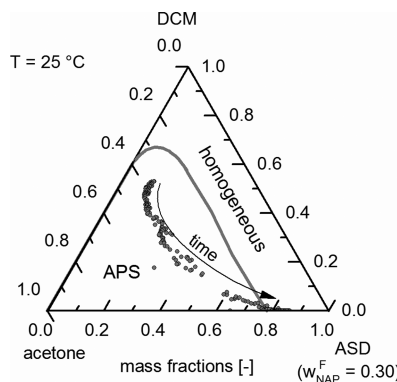


Figure 10. APS region for the quaternary system NAP/PVP/acetone/DCM evaluated for a NAP content of $w_{\text{NAP}}^{\text{F}} = 0.30$ in the solvent-free ASD. The gray solid line is the PC-SAFT-calculated turbidity line, and the points are experimentally determined data points during drying via Raman spectroscopy.

long as the mixture does not enter the APS region during drying.

Experimental Findings. Paudel et al.⁸ reported that the solvent selection to an unknown extent influenced the preparation of NAP/PVP ASDs using solvent evaporation from the solvent mixture acetone/DCM. In order to shed a light on these findings, exactly the same system was also investigated in this work. An NAP/PVP mixture with an NAP mass fraction of $w_{\text{NAP}}^{\text{F}} = 0.30$ was weighed and dissolved in an acetone/DCM mixture with $w_{\text{DCM}} = 0.60$ DCM. The NAP/PVP (commonly called ASD) weight fraction in the solvent mixture was $w_{\text{ASD}} = 0.05$. Approximately 100 μL of this mixture was casted on a glass cover slide, and the drying process was observed as a function of time. Photomicrographs showing the film at different time steps are shown in Figure 11.

At the start of the experiment, the quaternary solution was completely clear (Figure 11a). After 5 min of drying at room temperature (Figure 11b), this clear solution suddenly became cloudy. At the end of the experiment after 10 min (Figure 11c), droplet-like structures remained in the ASD film. A time-lapse video of the entire drying process is available in the Supporting Information. A time-dependent Raman investigation was conducted to further understand the reasons for the occurrence of turbidity during the experiment; the result of this measurement is illustrated in Figure 12 (and was already included as data points in Figure 10).

According to the first Raman spectrum (0 min), the initial solution contained 0.53 DCM, 0.35 acetone, 0.10 PVP, and 0.02 NAP. As can be seen in Figures 10 and 12, from the very

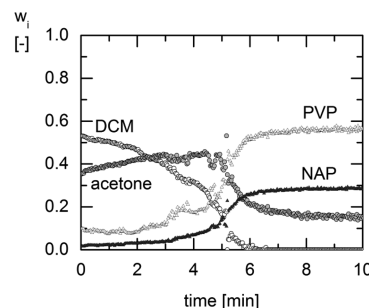


Figure 12. Investigation of the drying process of an NAP/PVP ASD prepared from a DCM/acetone mixture with Raman spectroscopy. The DCM mass fraction is represented by white circles, the acetone mass fraction by gray circles, the PVP mass fraction by white triangles, and the NAP mass fraction by gray triangles.

beginning, DCM evaporates faster than acetone due to the higher DCM vapor pressure compared to the vapor pressure of acetone. Thus, the weight fractions of the other components increase (the sum of all weight fractions always equals one). Therefore, acetone enriches during drying. After 4.8 min, the acetone concentration reached a maximum value of 0.44 and then began to decline as well. Just at this point of the measurement, the mass-fraction values of all four components began to scatter due to the starting phase separation in the sample, which is also to be seen in Figure 11b. DCM completely evaporated within 5.9 min, leaving behind a mixture of NAP/PVP/acetone with the already well-known APS region (Figure 7b). This measurement proved that solvents evaporate unevenly from a solvent mixture depending on their relative volatility. It moreover supplies a profound explanation for the occurrence of turbidity (phase separation) during the drying process and demonstrates that even clear starting mixtures might undergo APS during drying.

The fastest method to prepare ASDs via solvent evaporation is spray drying. Thus, in this work, NAP/PVP ASDs were also prepared via spray drying to check whether a manufacturing process with very rapid solvent evaporation could prevent APS in potentially demixing ASDs. The feed solution, which was already used for the drying experiment shown in Figures 11 and 12 (containing 0.015 NAP, 0.035 PVP, 0.57 DCM, and 0.38 acetone; numbers are mass fractions), was initially completely clear. Raman mapping experiments were not feasible for the obtained micro particles, thus DSC measurements were carried out to qualitatively investigate the physical state of the ASD after spray drying. The DSC reversing heat

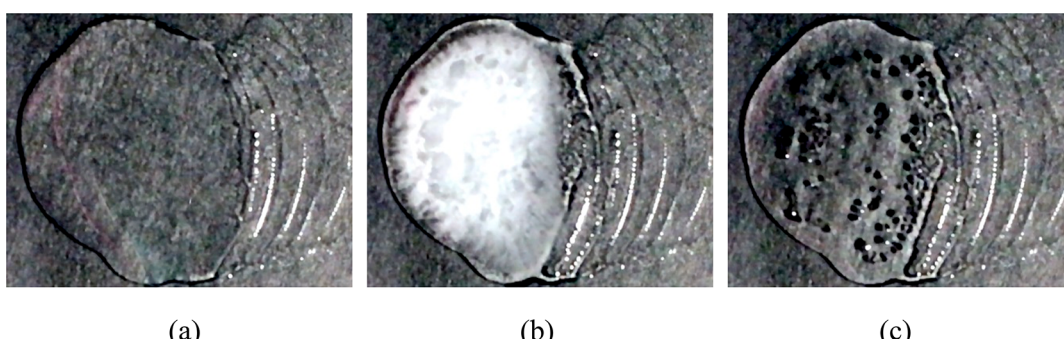


Figure 11. Photographs of a NAP/PVP/acetone/DCM droplet drying on a glass slide taken after (a) 0, (b) 5 min and (c) 10 min.

flow signals of the first and second heating ramps are shown in Figure 13.

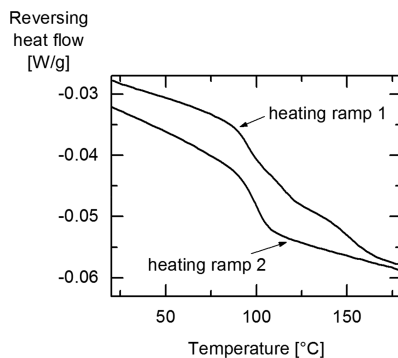


Figure 13. DSC reversing heat flow signal of a 30 wt % NAP/PVP ASD which was spray-dried using a mixture of $w = 0.40$ acetone and $w = 0.60$ DCM.

It can be seen, that during the first heating ramp of the spray-dried ASD, a corrugated heat flow signal was recorded. Various steps and crinkles are visible between 90 and 160 °C. In the second heating ramp, the heat flow signal shows a smooth and clear shape. The thermal history was removed in the second heating ramp, and now one clear glass transition temperature was observed at 100.9 °C (which perfectly agrees with earlier publications⁴³). From the corrugated first heat flow signal of the DSC measurement, it can be concluded that two amorphous phases with different API content were present in the spray-dried ASD, and APS thus also occurred during/after the fast solvent evaporation during spray drying. Remarkably, even fast drying techniques seem to be unable to prevent thermodynamically driven APS.

This finding dramatically emphasizes the importance of preventing APS during the preparation of an ASD, and that the choice of the appropriate solvent can hardly be overestimated. If one solvent is used to dissolve one compound (e.g., the polymer) and mixed with a second solvent used to dissolve the other compound (e.g., the API), a preferential evaporation of one of the solvents during drying might lead to APS. This can only be successfully prevented by choosing one solvent which dissolves both, API and polymer, at the same time. Only knowing the entire phase diagram of API/polymer/solvent mixtures allows for designing a feasible and reasonable production process of an ASD without occurring APS at any point of the process.

■ CONCLUSION

This work, for the first time, systematically investigated the phenomenon of APS occurring during the solvent-based preparation of ASDs. Thermodynamic predictions of the phase behavior, i.e., of API solubility in the polymer/solvent mixtures and of APS, were performed using the thermodynamic model PC-SAFT, and the glass transition of the ternary mixtures was predicted with the Gordon–Taylor equation.

According to the thermodynamic predictions and supported by the performed experiments, ethanol-based PVP ASDs were found to be completely miscible in the entire composition range, and ethanol is thus regarded as an “appropriate” solvent for the preparation of PVP-based ASDs. In contrast, acetone in combination with PVP undergoes APS and is thus regarded as an “inappropriate” solvent for preparing PVP-based ASDs.

Accordingly, dried NAP/PVP ASDs prepared using ethanol were found to be completely homogeneous, while those prepared using acetone showed drastic heterogeneities, which were characterized and quantified experimentally via Raman mapping and light microscopy.

It was thus shown that the solvent used for ASD preparation decisively influences the product homogeneity, although not being present anymore in the dry ASD. The reason for this could be identified in this work, namely, the immiscibility in the binary system polymer and solvent, which causes also an APS region in the API-containing system.

Different APIs (NAP and FEL) were compared to study their influence on the APS region. It was found from both, experimental results and thermodynamic predictions, that solvent-induced APS occurred regardless of the API as soon as the polymer/solvent system undergoes phase separation, yielding a sound explanation for the so far not understood phenomenon of APS.

Finally, acetone/DCM solvent mixtures were examined as possible alternatives for the preparation of PVP-based ASDs. Mixing acetone and DCM seemed to prevent APS at the first glance, since at the beginning of the drying process, this solvent mixture resulted in a clear API/PVP solution. However, thermodynamic predictions and corresponding experiments revealed an usually not-expected challenge when dealing with those mixtures. Upon drying, the ASD became turbid, again resulting in a heterogeneous ASD product. This phenomenon could be explained by the fact that the appropriate solvent DCM evaporated first, leaving behind a solution enriched in the nonappropriate solvent acetone and finally again leading to the unwanted APS. Spray-drying experiments revealed that even fast evaporation rates cannot prevent APS during drying.

Applying the thermodynamic modeling approach proposed in this work yields a completely new insight into the phenomenon of APS. It is able to explain the phenomenon of heterogeneous ASDs arising from the preparation methods using different solvents and solvent mixtures described in literature. It clearly shows that the choice of inappropriate solvents (like acetone in the case of PVP-containing ASDs), which are even not present in the dry ASD anymore, can cause product heterogeneities in the ASDs.

As pointed out in earlier studies,³¹ solvent-free NAP/PVP ASDs are fully miscible and show no APS. The NAP/PVP ASDs which underwent solvent-induced APS during the preparation (like those prepared using acetone or DCM/acetone mixtures) will also remix during storage. However, this process will take quite long since the heterogeneous ASD is below its glass transition after solvent removal. Thus, the ASD remains “frozen” in that metastable heterogeneous state for a very long time (even months or years). This means, that even thermodynamically stable (and thus finally homogeneous) polymer/API ASDs might erroneously experimentally be identified as being “unstable” since they were prepared using an inappropriate solvent and are not in their equilibrium state days or weeks after preparation.

By determining the thermodynamic phase equilibria as suggested by this work, it is possible to predict the occurrence of solvent-induced APS during ASD preparation and thus to identify suitable solvents and the best process conditions with minimum computational effort at early stages of process development.

■ ASSOCIATED CONTENT

● Supporting Information

The Supporting Information is available free of charge on the ACS Publications website at DOI: [10.1021/acs.molpharmaceut.8b00892](https://doi.org/10.1021/acs.molpharmaceut.8b00892).

Time lapse video of the drying process of a NAP/PVP ASD prepared using a DCM/acetone mixture ([AVI](#))

Solubility of crystalline APIs in organic solvents ([PDF](#))

■ AUTHOR INFORMATION

Corresponding Author

*Phone: +49 231 755 2635; Fax: +49 231 755 2572; E-mail: gabriele.sadowski@tu-dortmund.de.

ORCID

Christian Luebert: [0000-0001-5555-4965](#)

Gabriele Sadowski: [0000-0002-5038-9152](#)

Notes

The authors declare no competing financial interest.

■ ACKNOWLEDGMENTS

The authors would like to acknowledge the financial support from Deutsche Forschungsgemeinschaft (DFG) with Grant SA700/22-1. The authors thank Maximilian Wessner for initiating this work by accidentally choosing an “inappropriate” solvent for ASD preparation.

■ ABBREVIATIONS

API, active pharmaceutical ingredient; APS, amorphous phase separation; ASD, amorphous solid dispersion; DCM, dichloromethane; DSC, differential scanning calorimetry; FEL, felodipine; NAP, naproxen; PC-SAFT, perturbed-chain statistical associating fluid theory; PVP, poly(vinylpyrrolidone)

■ REFERENCES

- (1) Loftsson, T.; Brewster, M. E. Pharmaceutical applications of cyclodextrins: basic science and product development. *J. Pharm. Pharmacol.* **2010**, *62*, 1607–1621.
- (2) Chiou, W. L.; Riegelman, S. Pharmaceutical Applications of Solid Dispersion Systems. *J. Pharm. Sci.* **1971**, *60*, 1281–1302.
- (3) Dhirendra, K.; Lewis, S.; Udupa, N.; Atin, K. Solid dispersions: a review. *Pak. J. Pharm. Sci.* **2009**, *22*, 234–246.
- (4) van den Mooter, G. The use of amorphous solid dispersions: A formulation strategy to overcome poor solubility and dissolution rate. *Drug Discovery Today: Technol.* **2012**, *9*, e79–e85.
- (5) Vo, C. L.-N.; Park, C.; Lee, B.-J. Current trends and future perspectives of solid dispersions containing poorly water-soluble drugs. *Eur. J. Pharm. Biopharm.* **2013**, *85*, 799–813.
- (6) Vasconcelos, T.; Sarmento, B.; Costa, P. Solid dispersions as strategy to improve oral bioavailability of poor water soluble drugs. *Drug Discovery Today* **2007**, *12*, 1068–1075.
- (7) Leuner, C. Improving drug solubility for oral delivery using solid dispersions. *Eur. J. Pharm. Biopharm.* **2000**, *50*, 47–60.
- (8) Paudel, A.; van den Mooter, G. Influence of Solvent Composition on the Miscibility and Physical Stability of Naproxen/PVP K 25 Solid Dispersions Prepared by Cosolvent Spray-Drying. *Pharm. Res.* **2012**, *29*, 251–270.
- (9) Costa, E. D.; Priotti, J.; Orlandi, S.; Leonardi, D.; Lamas, M. C.; Nunes, T. G.; Diogo, H. P.; Salomon, C. J.; Ferreira, M. J. Unexpected solvent impact in the crystallinity of praziquantel/poly(vinylpyrrolidone) formulations. A solubility, DSC and solid-state NMR study. *Int. J. Pharm.* **2016**, *511*, 983–993.
- (10) Wu, J. X.; Yang, M.; van den Berg, F.; Pajander, J.; Rades, T.; Rantanen, J. Influence of solvent evaporation rate and formulation factors on solid dispersion physical stability. *Eur. J. Pharm. Sci.* **2011**, *44*, 610–620.
- (11) Wan, F.; Bohr, A.; Maltesen, M. J.; Bjerregaard, S.; Foged, C.; Rantanen, J.; Yang, M. Critical Solvent Properties Affecting the Particle Formation Process and Characteristics of Celecoxib-Loaded PLGA Microparticles via Spray-Drying. *Pharm. Res.* **2013**, *30*, 1065–1076.
- (12) Shultz, A. R.; Flory, P. J. Phase Equilibria in Polymer—Solvent Systems I, II. *J. Am. Chem. Soc.* **1952**, *74*, 4760–4767.
- (13) Koningsveld, R.; Staverman, A. J. Liquid–Liquid Phase Separation in Multicomponent Polymer Solutions. I. Statement of the Problem and Description of Methods of Calculation. *J. Polym. Sci. A-2 Polym. Phys.* **1968**, *6*, 305–323.
- (14) Koningsveld, R. Liquid–Liquid Equilibria in Multicomponent Polymer Systems. *Discuss. Faraday Soc.* **1970**, *49*, 144–161.
- (15) Walheim, S.; Böltau, M.; Mlynek, J.; Krausch, G.; Steiner, U. Structure Formation via Polymer Demixing in Spin-Cast Films. *Macromolecules* **1997**, *30*, 4995–5003.
- (16) Krause, S.; Iskandar, M. Phase Separation in Styrene- α -Methyl Styrene Block Copolymers. *Polymer Alloys* **1977**, *10*, 231–243.
- (17) Pappa, G. D.; Voutsas, E. C.; Tassios, D. P. Liquid–Liquid Phase Equilibrium in Polymer–Solvent Systems: Correlation and Prediction of the Polymer Molecular Weight and the Pressure Effect. *Ind. Eng. Chem. Res.* **2001**, *40*, 4654–4663.
- (18) van de Witte, P.; Dijkstra, P. J.; van den Berg, J. W. A.; Feijen, J. Phase separation processes in polymer solutions in relation to membrane formation. *J. Membr. Sci.* **1996**, *117*, 1–31.
- (19) Fischer, V.; Borchard, W.; Karas, M. Thermodynamic Properties of Poly(ethylene glycol)/Water Systems. I. A Polymer Sample with a Narrow Molar Mass Distribution. *J. Phys. Chem.* **1996**, *100*, 15992–15999.
- (20) Cocchi, G.; Angelis, M. G. D.; Sadowski, G.; Doghieri, F. Modelling polylactide/water/dioxane systems for TIPS scaffold fabrication. *Fluid Phase Equilibr.* **2014**, *374*, 1–8.
- (21) Flory, P. J. Thermodynamics of High Polymer Solutions. *J. Chem. Phys.* **1942**, *10*, 51–61.
- (22) Freed, K. F.; Dudowicz, J. Lattice Cluster Theory for Pedestrians: The Incompressible Limit and the Miscibility of Polyolefin Blends. *Macromolecules* **1998**, *31*, 6681–6690.
- (23) Gross, J.; Sadowski, G. Perturbed-Chain SAFT: An Equation of State Based on a Perturbation Theory for Chain Molecules. *Ind. Eng. Chem. Res.* **2001**, *40*, 1244–1260.
- (24) Mueller, F.; Naeem, S.; Sadowski, G. Toluene Sorption in Poly(styrene) and Poly(vinyl acetate) near the Glass Transition. *Ind. Eng. Chem. Res.* **2013**, *52*, 8917–8927.
- (25) Tumakaka, F.; Gross, J.; Sadowski, G. Modeling of polymer phase equilibria using Perturbed-Chain SAFT. *Fluid Phase Equilibr.* **2002**, *194–197*, 541–551.
- (26) Kleiner, M.; Tumakaka, F.; Sadowski, G.; Latz, H.; Buback, M. Phase equilibria in polydisperse and associating copolymer solutions: Poly(ethene-co-(meth)acrylic acid)—monomer mixtures. *Fluid Phase Equilibr.* **2006**, *241*, 113–123.
- (27) Reschke, T.; Brandenbusch, C.; Sadowski, G. Modeling aqueous two-phase systems: II. Inorganic salts and polyether homo- and copolymers as ATPS former. *Fluid Phase Equilibr.* **2014**, *375*, 306–315.
- (28) Ruether, F.; Sadowski, G. Modeling the Solubility of Pharmaceuticals in Pure Solvents and Solvent Mixtures for Drug Process Design. *J. Pharm. Sci.* **2009**, *98*, 4205–4215.
- (29) Cassens, J.; Prudic, A.; Ruether, F.; Sadowski, G. Solubility of Pharmaceuticals and Their Salts As a Function of pH. *Ind. Eng. Chem. Res.* **2013**, *52*, 2721–2731.
- (30) Paus, R.; Prudic, A.; Ji, Y. Influence of excipients on solubility and dissolution of pharmaceuticals. *Int. J. Pharm.* **2015**, *485*, 277–287.
- (31) Prudic, A.; Ji, Y.; Sadowski, G. Thermodynamic Phase Behavior of API/Polymer Solid Dispersions. *Mol. Pharmaceutics* **2014**, *11*, 2294–2304.

- (32) Luebbert, C.; Huxoll, F.; Sadowski, G. Amorphous-Amorphous Phase Separation in API/Polymer Formulations. *Molecules* **2017**, *22*, 296.
- (33) Lehmkemper, K.; Kyeremateng, S. O.; Heinzerling, O.; Degenhardt, M.; Sadowski, G. Long-Term Physical Stability of PVP- and PVPVA-Amorphous Solid Dispersions. *Mol. Pharmaceutics* **2017**, *14*, 157–171.
- (34) Lehmkemper, K.; Kyeremateng, S. O.; Heinzerling, O.; Degenhardt, M.; Sadowski, G. Impact of Polymer Type and Relative Humidity on the Long-Term Physical Stability of Amorphous Solid Dispersions. *Mol. Pharmaceutics* **2017**, *14*, 4374–4386.
- (35) Luebbert, C.; Sadowski, G. Moisture-induced phase separation and recrystallization in amorphous solid dispersions. *Int. J. Pharm.* **2017**, *S32*, 635–646.
- (36) Luebbert, C.; Klanke, C.; Sadowski, G. Investigating phase separation in amorphous solid dispersions via Raman mapping. *Int. J. Pharm.* **2018**, *S35*, 245–252.
- (37) Shamblin, S. L.; Zografi, G. The effects of absorbed water on the properties of amorphous mixtures containing sucrose. *Pharm. Res.* **1999**, *16*, 1119–1124.
- (38) Granberg, R. A.; Rasmussen, Å. C. Solubility of Paracetamol in Pure Solvents. *J. Chem. Eng. Data* **1999**, *44*, 1391–1395.
- (39) Tao, J.; Sun, Y.; Zhang, G. G. Z.; Yu, L. Solubility of Small-Molecule Crystals in Polymers: D-Mannitol in PVP, Indomethacin in PVP/VA, and Nifedipine in PVP/VA. *Pharm. Res.* **2009**, *26*, 855–864.
- (40) Hallbrucker, A.; Mayer, E.; Johari, G. P. The heat capacity and glass transition of hyperquenched glassy water. *Philos. Mag. B* **1989**, *60*, 179–187.
- (41) Lesikar, A. V. Effect of association complexes on the glass transition in organic halide mixtures. *J. Phys. Chem.* **1976**, *80*, 1005–1011.
- (42) Carpenter, M. R.; Davies, D. B.; Matheson, A. J. Measurement of the Glass-Transition Temperature of Simple Liquids. *J. Chem. Phys.* **1967**, *46*, 2451–2454.
- (43) Prudic, A.; Kleetz, T.; Korf, M.; Ji, Y.; Sadowski, G. Influence of Copolymer Composition on the Phase Behavior of Solid Dispersions. *Mol. Pharmaceutics* **2014**, *11*, 4189–4198.
- (44) Prudic, A.; Lesniak, A.-K.; Ji, Y.; Sadowski, G. Thermodynamic phase behaviour of indomethacin/PLGA formulations. *Eur. J. Pharm. Biopharm.* **2015**, *93*, 88–94.
- (45) Prausnitz, J. M.; Lichtenthaler, R. N.; Azevedo, E. G. d. *Molecular thermodynamics of fluid-phase equilibria*, 3rd ed.; Prentice-Hall international series in the physical and chemical engineering sciences; Prentice Hall PTR: Upper Saddle River, N.J., 1999.
- (46) Koningsveld, R. Phase Equilibria and Phase Separation: Proceedings of the 5th Polymer Meeting Point at the University of Essex. *Br. Polym. J.* **1975**, *7*, 435–458.
- (47) Lu, Q.; Zografi, G. Phase Behavior of Binary and Ternary Amorphous Mixtures Containing Indomethacin, Citric Acid and PVP. *Pharm. Res.* **1998**, *15*, 1202–1206.
- (48) Hancock, B. C.; Zografi, G. The Relationship Between the Glass Transition Temperature and the Water Content of Amorphous Pharmaceutical Solids. *Pharm. Res.* **1994**, *11*, 471–477.
- (49) Paudel, A.; van Humbeeck, J.; van den Mooter, G. Theoretical and Experimental Investigation on the Solid Solubility and Miscibility of Naproxen in Poly(vinylpyrrolidone). *Mol. Pharmaceutics* **2010**, *7*, 1133–1148.
- (50) Paus, R.; Ji, Y.; Braak, F.; Sadowski, G. Dissolution of Crystalline Pharmaceuticals: Experimental Investigation and Thermo-dynamic Modeling. *Ind. Eng. Chem. Res.* **2015**, *54*, 731–742.
- (51) Marsac, P. J.; Li, T.; Taylor, L. S. Estimation of Drug-Polymer Miscibility and Solubility in Amorphous Solid Dispersions Using Experimentally Determined Interaction Parameters. *Pharm. Res.* **2009**, *26*, 139–151.
- (52) Tumakaka, F.; Sadowski, G. Application of the Perturbed-Chain SAFT equation of state to polar systems. *Fluid Phase Equilib.* **2004**, *217*, 233–239.
- (53) Tihic, A.; Kontogeorgis, G. M.; von Solms, N.; Michelsen, M. L. Applications of the simplified perturbed-chain SAFT equation of state using an extended parameter table. *Fluid Phase Equilib.* **2006**, *248*, 29–43.
- (54) Gross, J.; Sadowski, G. Application of the Perturbed-Chain SAFT Equation of State to Associating Systems. *Ind. Eng. Chem. Res.* **2002**, *41*, 5510–5515.
- (55) Wolbach, J. P.; Sandler, S. I. Using Molecular Orbital Calculations To Describe the Phase Behavior of Cross-associating Mixtures. *Ind. Eng. Chem. Res.* **1998**, *37*, 2917–2928.
- (56) Prudic, A. Phase behavior of polymer based pharmaceutical formulations. *Thermodynamik*; Verlag Dr. Hut: München, 2016.
- (57) Caßens, J. Modellierung thermodynamischer Eigenschaften pharmazeutischer Substanzen in Lösungsmitteln und Lösungsmittelgemischen. *Thermodynamik*; Dr. Hut: München, 2013.
- (58) Krüger, K.-M.; Sadowski, G. Fickian and Non-Fickian Sorption Kinetics of Toluene in Glassy Polystyrene. *Macromolecules* **2005**, *38*, 8408–8417.
- (59) Alsmeyer, F.; Koss, H.-J.; Marquardt, W. Indirect Spectral Hard Modeling for the Analysis of Reactive and Interacting Mixtures. *Appl. Spectrosc.* **2004**, *58*, 975–985.
- (60) Kriesten, E.; Alsmeyer, F.; Bardow, A.; Marquardt, W. Fully automated indirect hard modeling of mixture spectra. *Chemom. Intell. Lab. Syst.* **2008**, *91*, 181–193.
- (61) Zafarani-Moattar, M. T.; Samadi, F. Determination of Solvent Activity in Poly(vinylpyrrolidone) + Methanol, + Ethanol, + 2-Propanol, + and 1-Butanol Solutions at 25 °C. *J. Chem. Eng. Data* **2004**, *49*, 1475–1478.